Paper accepted for publication in International Journal of Rail Transportation, journal DOI: 10.1080/23248378.2022.2106599

The effect of rail shields on railway rolling noise

Xianying Zhang*[1, 2], David Thompson[2], Jungsoo Ryue[3], Hongseok Jeong[4], Giacomo Squicciarini[2]

[1]*College of Transportation Engineering, Tongji University, Shanghai, 201804, China*

[2]*Institute of Sound and Vibration Research, University of Southampton, Southampton SO17 1BJ, UK*

[3]*School of Naval Architecture and Ocean Engineering, University of Ulsan, Ulsan 44610, South Korea*

[4]*Korea Research Institute of Ships and Ocean Engineering, Daejeon 34103, South Korea*

Email: xianyingzhang@tongji.edu.cn

Abstract

Rail shields have been developed recently which are fitted around the lower part of the rail and are intended to reduce the noise radiated by the rail. Their effect on the sound radiation is investigated theoretically by using a 2.5D finite element / boundary element approach including the acoustic effects of the ground. The insertion loss due to the rail shields is predicted and compared with available measured data and the most important features of the shields are identified. The overall noise reduction when applied to railway track is determined by combining the numerical results with estimates of rolling noise from the TWINS model. The rail shields are effective in the middle frequency range, where the rail is the most important noise source. The overall A-weighted sound level is reduced by 2-3 dB for a track with soft rail pads, and 1-2 dB for a track with stiff pads.

Keywords: railway rolling noise; track noise reduction; acoustic shielding; 2.5D methods

1. Introduction

The most important source of environmental noise from railways at conventional speeds is rolling noise. This is produced by the vibration of the track and wheels, which is induced by their combined surface roughness at the wheel/rail contact [1]. The relative importance of the wheel and track radiation depends on the details of their design, the roughness spectrum and the train speed [1]. Nonetheless, the component of noise radiated by the rail is often the highest, and dominates the important mid-frequency region between 400 and 2000 Hz.

Trackside barriers are commonly used to reduce the environmental noise from railways. However, these are expensive and also visually intrusive and may therefore be opposed by local communities. Beier et al. [2] showed that low noise barriers close to the track may reduce noise by up to 7 dB, but this depends on the height of the barrier, the distance to the noise source and the location of the receiver point.

Control of noise at source is often a more cost-effective and attractive alternative. Various techniques to control rolling noise have been trialled in recent years, as summarised for example in [2, 3, 4]. Focussing on the track noise radiation, a number of designs of rail damper have been developed [5, 6, 7]. They reduce the noise from the rail by increasing the track decay rate to reduce the average vibration of the rail. An overall noise reduction of up to 4 dB(A) was obtained in field tests presented in [8]. In other situations, depending on the rail pad stiffness, the noise reduction is found to be between 1 and 3 dB(A) [2, 4].

As an alternative, a rail shield has been proposed which covers the rail web in an attempt to block its sound radiation [9]. This consists of a thin metal plate surrounding the rail web and foot. A constrained layer damping treatment is applied to the plate and absorptive material is included inside the shield. The mechanism of noise reduction is different from a rail damper as, unlike rail dampers, these shields do not influence the track decay rate significantly but instead reduce the radiated sound due to a given vibration level [9]; measured noise reductions of 2 to 4 dB were obtained on a ballasted track in Austria. Field tests in Germany have identified a noise reduction of up to 3 dB(A), dependent on the type of train [2]. Further information on these rail shields was given in [10] including the installation procedure. Measurements in situ in Switzerland showed that a reduction in the pass-by noise level in the range of 1-4 dB could be achieved. Its greatest effect occurred when the contribution of the rail dominated the rolling noise.

To characterize the effect on the sound radiation of this kind of rail shield, Dittrich et al. [11] performed measurements on a dedicated test track by exciting the rail using hammer excitation in the lateral and vertical directions; reciprocal measurements were also carried out using acoustic excitation. The shields were found to be most effective for the lateral excitation of the rail [11].

The vibration of railway track has been widely studied [1]. It consists predominantly of waves in the rail [12], which propagate at frequencies above their cut-on frequency; this frequency is determined by the resonance of the rail mass on the rail pad stiffness. At low frequencies vertical and lateral bending and torsional waves propagate; above 1 kHz higher order waves also cut on which contain cross-sectional deformation [13, 14].

To understand the generation of rolling noise, theoretical models have been developed. The TWINS model [15] has become established as a state-of-the-art engineering model, and has been validated against extensive field measurements [16, 17]. More recently, Zhang et al. [18] studied the effect of the acoustic boundary conditions of the rail on its sound radiation using a 2D boundary element approach. The model in [15] was based on the assumption that the rail can be considered to radiate into a free field, the results from which take the form of a line dipole. Zhang et al. [18] showed that a rail attached to a rigid ground radiates like a line monopole, which gives increased sound power at low frequency, whereas a rail located at a small distance above the ground (reflective or absorptive) radiates like a line quadrupole. These conclusions were validated against laboratory measurements on a 1:5 scale rail. An appropriate combination of these conditions has been shown to give a good approximation to the 3D behaviour of a rail installed in the track [19]. An improved model for the sleeper radiation was

also presented in [20] which takes account of the acoustic interaction between multiple sleepers. The properties of ballast as an absorptive medium were discussed in [21].

An alternative approach to predict the rail radiation is to use the waveguide finite element and boundary element (WFE/BE) methods, also known as 2.5D methods [22]. Nilsson et al. [23] studied the sound radiation from a rail using this approach and compared the behaviour of an 'open' rail in free field with an embedded rail. Ryue et al. [24] included the ground in this approach and Sun et al. [25] studied embedded rails in more detail. As the radiating length of the rail is of the order of tens of metres, the 2.5D approach is much more efficient than a full 3D FE/BE approach, e.g. [26].

In practice, railway tracks have discrete supports, which can introduce effects such as the pinned-pinned resonances [1]. The most important pinned-pinned resonance occurs typically around 1 kHz for the vertical direction, and higher order pinned-pinned modes also occur. There can be large variations in the vertical point mobility of the track around the pinned-pinned frequencies, especially for stiffer rail pads [1, 27, 28]. There are also similar pinned-pinned phenomena in the lateral direction, although their effect is much less pronounced.

In [29], discrete supports were introduced into a 2.5D model of the rail by coupling it to discrete sleepers using a receptance coupling technique. Theyssen et al. [30] used a similar technique to model the vibration of a slab track and also predicted the sound radiation using a 2.5D boundary element model.

Despite the potentially large variations in point mobility, the average noise during a train pass-by is affected to a much smaller extent by the presence of discrete supports. In Section 3.4.1 of [1], the differences between continuous and discrete supports are shown in terms of the rail vibration, averaged over a length of ±20 m and averaged over 12 force positions within a sleeper span. This quantity is directly correlated with the noise radiated by the rail. Differences between continuous and discretely supported models were restricted to a narrow frequency region in the vicinity of 1 kHz where the difference in one-third octave bands was at most 1.4 dB. The TWINS model for rolling noise is usually based on a track vibration model with an equivalent continuous support, but despite this limitation, extensive validation of the TWINS model [15, 16, 17] has shown that good agreement is obtained with measurements of noise.

The aim of this paper is to study the mechanisms of the sound reduction obtained with a rail shield, by making use of the 2.5D FE/BE method. Although the analysis is based roughly on the design concept presented in [9], it is not the intention to represent the behaviour of a particular product in detail, but rather to study the generic behaviour of such a shield. A preliminary study has been presented in [31] but this did not take account of the proximity of the ground. The present work therefore extends this study to include the effects of the ground and to investigate the dependence on various parameters describing the shields.

Section 2 briefly summarises the WFE/BE methods used in this paper. The sound radiation from a rail, including the ground effects, is presented in Section 3 using the WFE/BE methods. The sound radiation in the presence of a rail shield is presented in Section 4 and the results are compared with measured data from [11]. The dependence on various parameters is studied in Section 5 to investigate the main reasons for the noise reduction. In Section 6, the predicted

noise reductions achieved by the rail shields are combined with rolling noise estimates obtained using TWINS for two typical railway tracks and two different wheel designs. Section 7 finally summarises the conclusions.

2. Waveguide finite element and boundary element method

The waveguide finite element and boundary element (WFE/BE) approaches used in this study have been described in detail in [18, 19, 23]. For clarity they are briefly summarised here. For the analysis in this paper, a software program WANDS is used [22].

A structure which is invariant in one direction, here denoted the *x*-direction, and has an arbitrary cross-section in the (*y*, *z*) plane, can be discretised in a conventional way using finite elements in this plane. For the WFE analysis, the partial differential equation of the structure is given by

$$\left[\mathbf{K_2}\frac{\partial^2}{\partial x^2} + \mathbf{K_1}\frac{\partial}{\partial x} + \mathbf{K_0} - \mathbf{M}\frac{\partial^2}{\partial t^2}\right]\mathbf{U}(x,t) = \mathbf{F}(x,t) \tag{1}$$

where $\mathbf{K_2}$, $\mathbf{K_1}$ and $\mathbf{K_0}$ are stiffness matrices and $\mathbf{M}$ is the mass matrix of the cross-section; $\mathbf{U}(x, t)$ is the vector of displacements of FE node points on the cross-section and $\mathbf{F}$ is the corresponding external force vector. If plate or beam elements are employed, a fourth order differential term $\mathbf{K_4}\partial^4/\partial x^4$ is added at the left-hand side of Equation (1). Since the structure remains invariant in the *x* direction, all the matrices in the equation are independent of *x*. By assuming a harmonic dependence with respect to time with frequency ω and with respect to the *x* coordinate with wavenumber k_x, the displacement vector can be written as $\mathbf{U}(x,t) = \tilde{\mathbf{U}}e^{\mathrm{i}(\omega t - k_x x)}$. Equation (1) then becomes

$$[\mathbf{K_2}(-\mathrm{i}k_x)^2 + \mathbf{K_1}(-\mathrm{i}k_x) + \mathbf{K_0} - \omega^2\mathbf{M}]\tilde{\mathbf{U}} = \tilde{\mathbf{F}} \tag{2}$$

where $\tilde{\mathbf{U}}$ and $\tilde{\mathbf{F}}$ contain the displacement amplitudes of the nodes and the corresponding amplitudes of the external forces in the wavenumber domain.

In addition, acoustic waveguide finite elements can be used for modelling interior spaces. These are included in the formulation in Equation (2). To represent porous materials, a poro-elastic finite element model [32, 33] has been introduced into the WANDS software based on Biot's poro-elasticity equations [34]. This can be coupled with both the solid and fluid finite element domains.

When the exterior of the waveguide structure is coupled with a fluid domain, waveguide boundary elements can be introduced to the periphery of the structure to model the external fluid. For a given frequency ω and wavenumber k_x, the governing equation for the external fluid is written as

$$\mathbf{H}(k_n)\tilde{\boldsymbol{\psi}} - \mathbf{G}(k_n)\frac{\partial\tilde{\boldsymbol{\psi}}}{\partial \mathrm{n}} = \mathbf{0} \tag{3}$$

where **H** and **G** are matrices of acoustic Green's functions; $\tilde{\boldsymbol{\psi}}$ and $\frac{\partial\tilde{\boldsymbol{\psi}}}{\partial \mathrm{n}}$ are vectors of the velocity potential and the normal velocity at the nodes of the boundary elements and **n** is the unit normal vector of the WBEs, pointing out of the acoustic domain. For exterior problems in the boundary

element method, 'CHIEF' points are used to overcome the non-uniqueness problem associated with resonances of the corresponding interior problems [35].

The wavenumber k_n in the (y, z) plane in Equation (3) is given by

$$k_n = \sqrt{k_a^2 - k_x^2} \tag{4}$$

where $k_a = \omega/c_0$ is the acoustic wavenumber and c_0 is the acoustic wave speed. If $k_a \geq k_x$, k_n is a real value and the structure can radiate sound into the far field, whereas if $k_a < k_x$, k_n is imaginary and the solution will consist of a near field radiating no sound power to the far field.

For the coupling between WFE and WBE, the pressure from the fluid is applied as an additional load to the structure; the coupled WFE equation is then written as

$$[\mathbf{K_2}(-\mathrm{i}k_x)^2 + \mathbf{K_1}(-\mathrm{i}k_x) + \mathbf{K_0} - \omega^2\mathbf{M}]\tilde{\mathbf{U}} - \mathrm{i}\omega\rho_0\mathbf{C_1}\tilde{\boldsymbol{\Psi}} = \tilde{\mathbf{F}} \tag{5}$$

where $\mathbf{C}_1$ denotes a coupling matrix associating the coupled degrees of freedom (dofs) between the WFE and WBE and ρ_0 is the fluid density. The velocity continuity condition at the interface between the WFE and WBE is written as

$$\mathbf{I_2}\frac{\partial\tilde{\boldsymbol{\Psi}}}{\partial\mathbf{n}} = \mathrm{i}\omega\rho_0\mathbf{C_2}\tilde{\mathbf{U}} \tag{6}$$

where $\mathbf{I}_2$ and $\mathbf{C}_2$ are matrices allocating coupled dofs in $\frac{\partial\tilde{\boldsymbol{\Psi}}}{\partial\mathbf{n}}$ and $\tilde{\mathbf{U}}$, respectively. For the WBE uncoupled with WFE, boundary conditions need to be specified. The boundary condition for each uncoupled node point in WBE can be defined in the wavenumber domain as

$$C_a\tilde{p} + C_b\tilde{v}_n = C_c \tag{7}$$

where $\tilde{p}$ and $\tilde{v}_n$ denote the sound pressure and the fluid particle velocity in the normal direction [36]. For example, the WBE nodes having a locally reactive impedance (z_n) condition can be specified by giving

$$C_a = 1,\ C_b = -z_n,\ C_c = 0 \tag{8}$$

The sound pressure and normal velocity are obtained from the velocity potential by

$$\tilde{\boldsymbol{p}} = \mathrm{i}\omega\rho_0\tilde{\boldsymbol{\Psi}},\ \tilde{\boldsymbol{v}}_n = -\frac{\partial\tilde{\boldsymbol{\Psi}}}{\partial\mathbf{n}} \tag{9}$$

Equation (7) can be written in matrix form as

$$\mathrm{i}\omega\rho_0\mathbf{C_a}\tilde{\boldsymbol{\Psi}} - \mathbf{C_b}\frac{\partial\tilde{\boldsymbol{\Psi}}}{\partial\mathbf{n}} = \mathbf{C_c} \tag{10}$$

Combining Equations (5-7) and (10), the governing equation of the coupled WFE/WBE system is expressed as

$$\begin{bmatrix} \mathbf{K}-\omega^2\mathbf{M} & -\mathrm{i}\omega\rho_0\mathbf{C_1} & \mathbf{0} \\ \mathbf{0} & \mathbf{H} & -\mathbf{G} \\ -\mathrm{i}\omega\rho_0\mathbf{C_2} & \mathbf{0} & \mathbf{I_2} \\ \mathbf{0} & \mathrm{i}\omega\rho_0\mathbf{C_a} & -\mathbf{C_b} \end{bmatrix} \begin{pmatrix} \tilde{\mathbf{U}} \\ \tilde{\boldsymbol{\Psi}} \\ \frac{\partial\tilde{\boldsymbol{\Psi}}}{\partial\mathbf{n}} \end{pmatrix} = \begin{pmatrix} \tilde{\mathbf{F}} \\ \mathbf{0} \\ \mathbf{0} \\ \mathbf{C_c} \end{pmatrix} \tag{11}$$

where $\mathbf{K} = \mathbf{K_2}(-\mathrm{i}k_x)^2 + \mathbf{K_1}(-\mathrm{i}k_x) + \mathbf{K_0}$. The coupled structural and acoustic response can be obtained by solving this equation.

The sound power radiated from the structure can be determined by integrating over the wavenumber domain

$$W = \frac{1}{4\pi}\mathrm{Re}\left(\int_{-k_a}^{k_a}\int_{\Gamma} \tilde{p}^*(k_x)\tilde{v}_n(k_x)\mathrm{d}\Gamma\,\mathrm{d}k_x\right) \tag{12}$$

where * denotes the complex conjugate and Γ is the perimeter of the cross-section in contact with the fluid. Since sound power can only be radiated from the structure when $|k_x| \leq k_a$, the integration with respect to k_x in Equation (12) is limited to $-k_a \leq k_x \leq k_a$.

3. The sound radiation from a rail in proximity with the ground

The sound radiation of a rail of type CEN 60E2 in close proximity to the ground is first investigated here as a reference case. This is modelled in the 2.5D finite element / boundary element software WANDS [22] using a similar modelling approach to that described in [23, 24]. The mesh used for the rail cross-section is shown in Figure 1(a) and the material properties used are listed in Table 1. In the structural model the rail is supported on a single layer of elements representing the rail pad (shaded in the figure). This is assigned orthotropic material properties to ensure that the pad stiffnesses in vertical and lateral directions correspond to those listed in Table 1. Both soft pads and stiff pads will be studied. In the structural model an equivalent continuous support is used; the stiffnesses per unit length are those given in Table 1 divided by the nominal fastener spacing of 0.6 m.

As discussed in the introduction, extensive experimental validation of rolling noise predictions [15, 16, 17] has shown that, despite adoption of a continuous support in the model, good agreement is obtained with measurements of noise. In the current study these discrete support effects on the vibration are therefore neglected, in common with the approach usually adopted in the TWINS model [15, 16]. This omission is expected to have minimal effect on the results, especially where these are shown in terms of the insertion loss of the rail shields.

Three different sets of acoustic boundary conditions are considered for the sound radiation calculations. The first is a free rail, in which acoustic boundary elements are located on the perimeter of the rail, including the bottom of the rail foot, thus neglecting the rail pad in the acoustic model (although it is included in the vibration part of the model); these elements are shown in red in Figure 1(a). Second, to represent the region of the rail above the sleepers, the rail is considered attached to the sleeper, as shown in Figure 1(b). Here a symmetry plane is used for the ground and the boundary elements do not enclose the rail foot. Third, to represent the region between sleepers, the rail is located above a partially absorptive ground plane representing the ballast, see Figure 1(c), where the distance between the rail foot and the ground surface is assumed to be 50 mm. The boundary elements enclose the rail as in the first model; additionally, a box is introduced to represent the ground with an impedance boundary condition on its upper surface [18]. The box dimensions used are the same as those in [18], and the box height is 0.5 m.

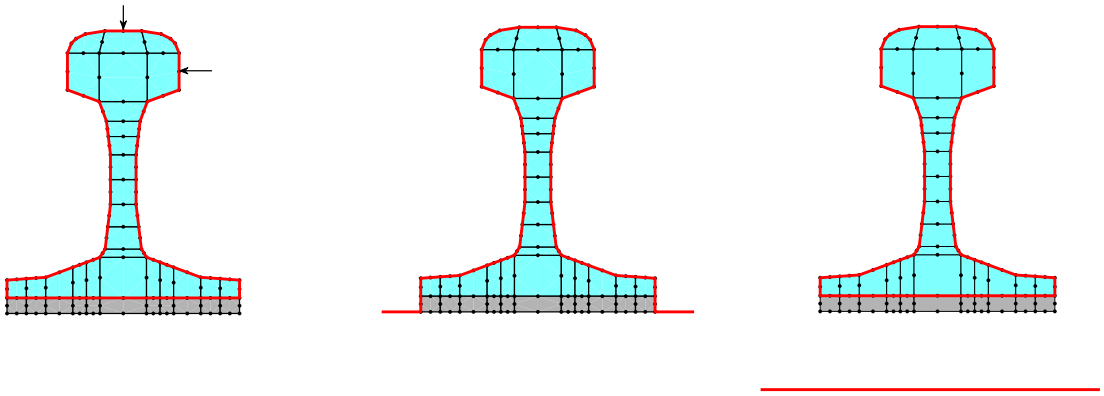

(a) (b) (c)

Figure 1 Mesh of the cross-section of a rail including the ground. (a) Free rail; (b) Rail attached to a ground; (c) Rail above a ground. Grey shaded region represents the rail pad (not included in the boundary element model). Thick red lines represent acoustic boundary elements.

Table 1 Parameters used for the 2.5D rail model

Rail		
Young's modulus	2.1×10^{11} N/m^2	
Poisson's ratio	0.3	
Density	7850 kg/m^3	
Damping loss factor	0.02	
Rail pad	Vertical	Lateral
Stiffness (soft pad)	150 MN/m	25 MN/m
Stiffness (stiff pad)	800 MN/m	66 MN/m
Damping loss factor	0.2	0.2

To account for rail cross-section deformation, which could be important for the behaviour of a rail shield, a unit force is applied to the rail head: this is located at the centre in the vertical direction or at the middle of the side in the lateral direction, as shown in Figure 1(a). The results are calculated for the frequency range from 40 to 6300 Hz, with a logarithmic spacing and 50 points per decade. This model does not include the vibration of the sleepers which would modify the vertical response below about 300 Hz [1].

The sound power radiated by the rail is calculated for a unit force, as described above. This result is then normalised by half the squared point mobility. This represents the sound power for a unit mean-square velocity at the excitation point [23].

The results with the soft pad for the three cases indicated in Figure 1 are shown in Figure 2 for each direction. For the vertical excitation of the rail, the differences due to the acoustic boundary conditions are greatest below 400 Hz [18] whereas for the lateral direction the ground has a smaller effect. These results are used as the reference for the subsequent calculations of the effect of rail shielding in the following sections. The results from the rail attached to a rigid ground and above an absorptive ground can be combined following the method proposed in

[19]. This simulates the periodic conditions of the rail attached to sleepers and above absorptive ground between them.

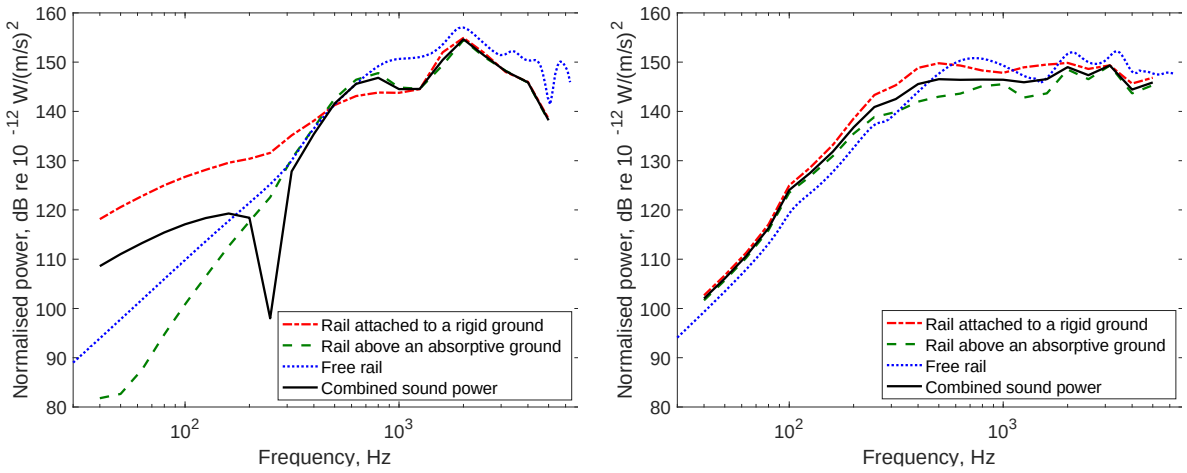

Figure 2 Sound power from the rail with different acoustic boundary conditions. (a) Vertical excitation; (b) Lateral excitation

4. The sound radiation from a rail with acoustic shields

To model the rail shield mounted on the rail, the same three acoustic boundary conditions are used, as described above for the unshielded rail. The effect of the shields on the sound radiation is explored in this section.

4.1 Modelling a rail fitted with acoustic shields

The sound radiation of the CEN 60E2 rail fitted with shields is calculated by using the same 2.5D FE/BE approach. The geometry of this shield is determined by the following constraints: the top of the shield is 30 mm below the outer corner of the rail head and at the base it is 10 mm away from the rail foot in the lateral direction (also 10 mm below the bottom of the rail foot). The plate is assumed to be steel with a thickness of 1 mm, which gives it a mass that is consistent with that cited in [11]. Its damping loss factor is chosen to be 0.5 which is indicative of a highly damped plate. The sensitivity of the results to these assumptions will be examined in Section 5.

In a practical installation some porous absorbing material may be included inside the shield [11]. To simulate this effect, a region of poro-elastic finite elements has been included in the model, and the corresponding mesh is shown in Figure 3. In Figure 3(a) the rail with shields is located above the ballast, whereas in Figure 3(b) it is directly above the sleeper surface, where the bottom of the shield is neither connected to the ground in the vibration model nor connected to the air in the acoustic model.

The model in Figure 3 is a fully coupled FE/BE model, in which the vibration of the rail and the shield are coupled with the acoustic fluid inside and outside the shield and within the poro-

elastic medium. The model therefore takes full account of the sound radiation from vibration of the shield as well as the rail.

In the model, the rail vibration is again calculated when it is continuously supported on a layer of elements representing the rail pads; rail and rail pads are modelled using solid finite elements as before. The rail pads are not shown in Figure 3 but are superimposed on the porous material beneath the rail foot. The shield is modelled by using a continuous plate reaching from the rail web to the underside of the foot. Its upper edge is mechanically coupled to the rail web in translation (vertically and laterally) but is allowed to rotate freely at the connection point. The air inside the shield is represented by using acoustic finite elements. The maximum element size in the fluid region is 2 cm which gives five node points per acoustic wavelength at the maximum frequency. The shaded elements shown correspond to the poro-elastic material. This extends beneath the rail foot as well as being located on the sides of the shield. It is dynamically coupled to both the rail foot and the shield, and is assumed to co-exist with the rail pad. The properties used for this porous material correspond to a typical melamine foam [32] and are listed in Table 2.

For the case above the sleeper surface, gaps are required in the shields around the rail fasteners. Although these discrete gaps at each sleeper cannot be modelled directly using a 2.5D approach, an estimate of their effect is obtained by introducing an equivalent continuous gap into the shield with a similar area per sleeper bay as may be found in practice. The corresponding mesh with the gap in the shield is shown in Figure 3(b), where the fluid domain on the inside is coupled directly to the exterior boundary element domain over a length of 17 mm on each side, as indicated by the asterisks. The plate elements still exist in this region to provide a connection between upper and lower shield regions but they are not connected to the fluid.

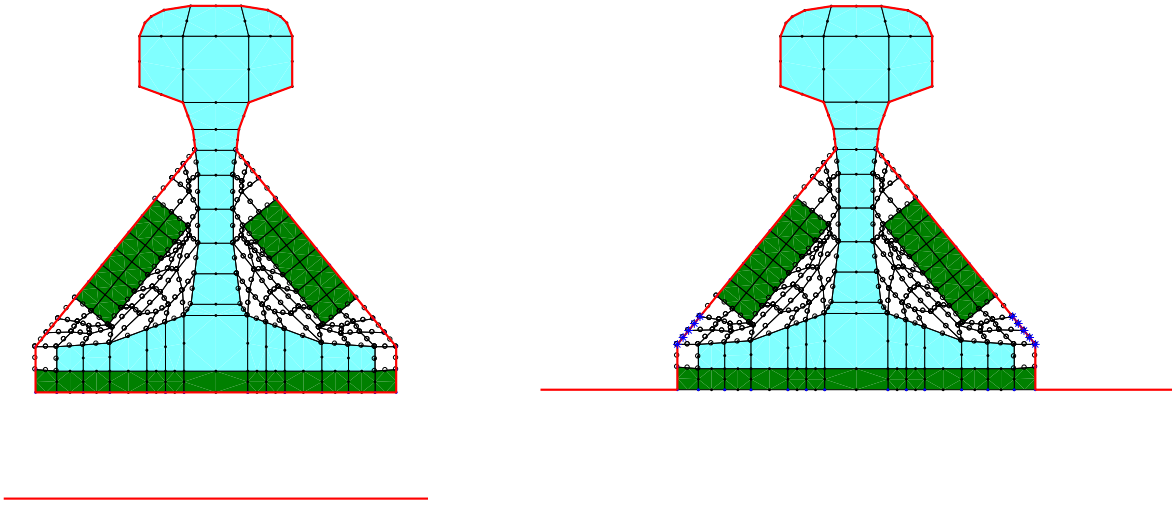

Figure 3 Mesh of rail cross-section with shield including porous absorbing material (elements with dark shaded area). (a) rail with shields above the ground (without gaps); (b) rail with shields attached to the sleeper/ground (with gaps indicated by asterisks).

Table 2 Parameters used for the acoustic shields

Shield	
Young's modulus	2.1×10^{11} N/m^2
Poisson's ratio	0.3
Density	7850 kg/m^3
Damping loss factor	0.5
Thickness	1 mm
Air	
Sound speed	343 m/s
Density	1.21 kg/m^3
Damping loss factor	0.001
Porous material	
Porosity	0.97
Flow resistivity	11000 Pa.s/m^2
Tortuosity	1.06
Viscous characteristic length	100 μm
Thermal characteristic length	200 μm
Young's modulus	1.22×10^5 N/m^2
Poisson's ratio	0.42
Density	11 kg/m^3
Damping loss factor	0.15

4.2 Calculation results

Before the analysis of the sound radiation from the rail with shields, the decay rate of the track with and without shields has been determined for both vertical and lateral excitation by using the procedure in EN 15461 [37]. The track decay rate is shown in Figure 4 for the track with soft pads. As expected from [9], the shield does not modify the track decay rate due to its low mass and stiffness compared with the rail. The point mobilities, not shown, are also unaffected by the presence of the shields.

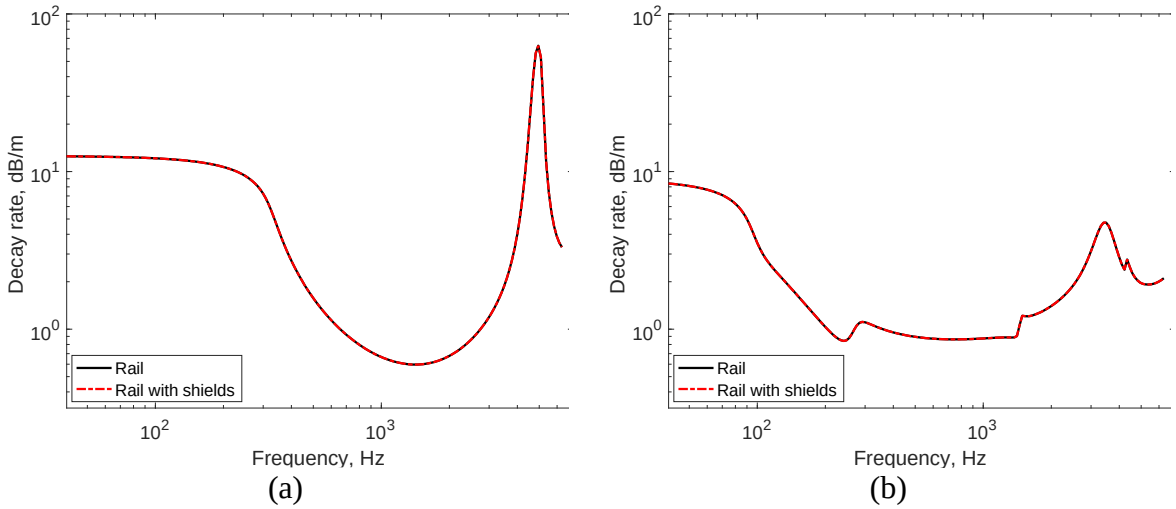

Figure 4 Comparison of the track decay rate. (a) Vertical excitation; (b) Lateral excitation

Examples of the deflected shape of the rail are shown in Figures 5 and 6. Figure 5 shows the rail deflected shapes in the main vertical bending wave, with and without the shield, at four example frequencies, whereas Figure 6 shows the corresponding results for lateral excitation of the rail. As can be seen, the rail vibration changes little due to the addition of the shields.

Although the vibration of the shield can be relatively large at some frequencies, e.g. at 1 kHz in the lateral direction, the wavelength is quite short which will mean that the radiation from the shield can be expected to be inefficient.

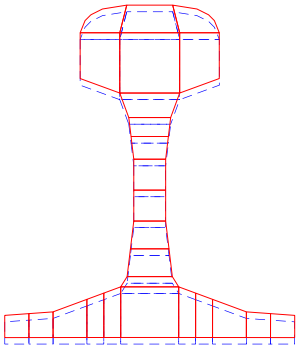

(a)

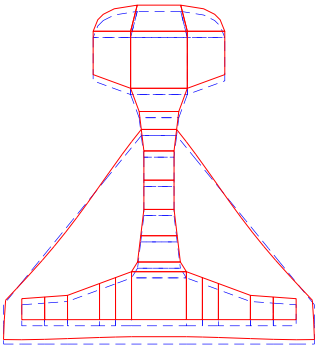

(e)

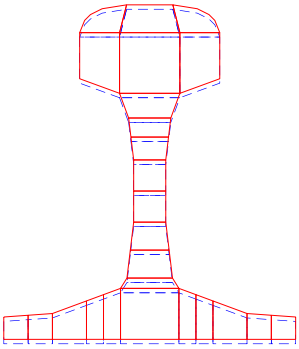

(b)

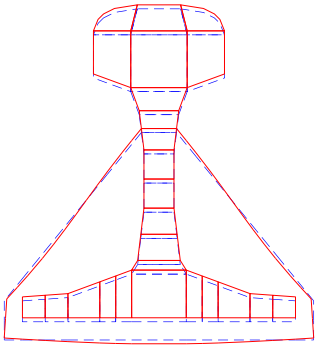

(f)

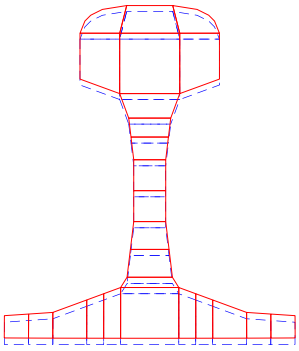

(c)

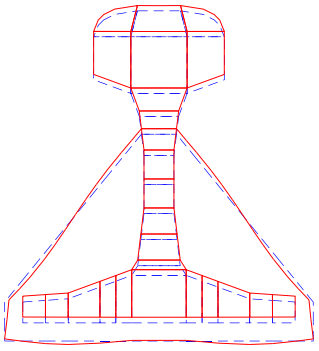

(g)

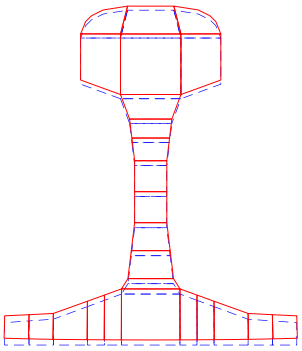

(d)

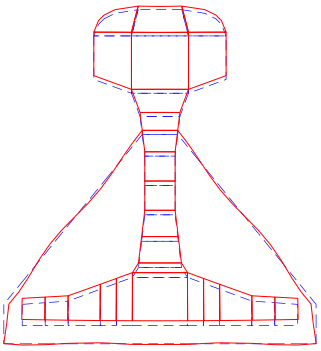

(h)

Figure 5 Examples of rail deflected shapes (exaggerated amplitude) for vertical excitation of the rail head. Left: rail without shield: (a) 250 Hz; (b) 500 Hz; (c) 1000 Hz; (d) 2000 Hz. Right: rail with shields fitted: (e) 250 Hz; (f) 500 Hz; (g) 1000 Hz; (h) 2000 Hz.

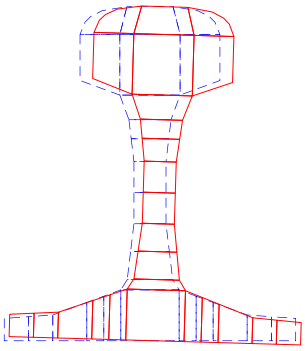

(a)

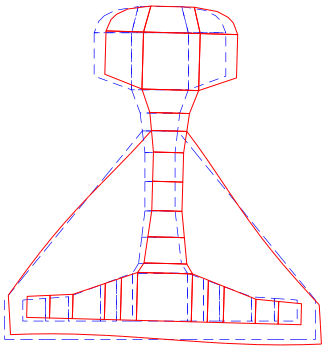

(e)

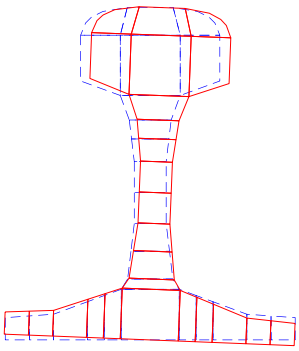

(b)

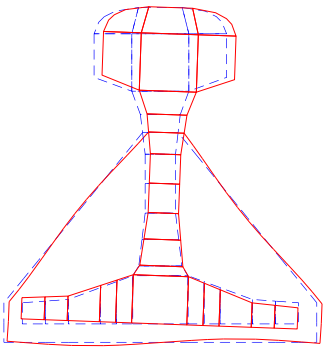

(f)

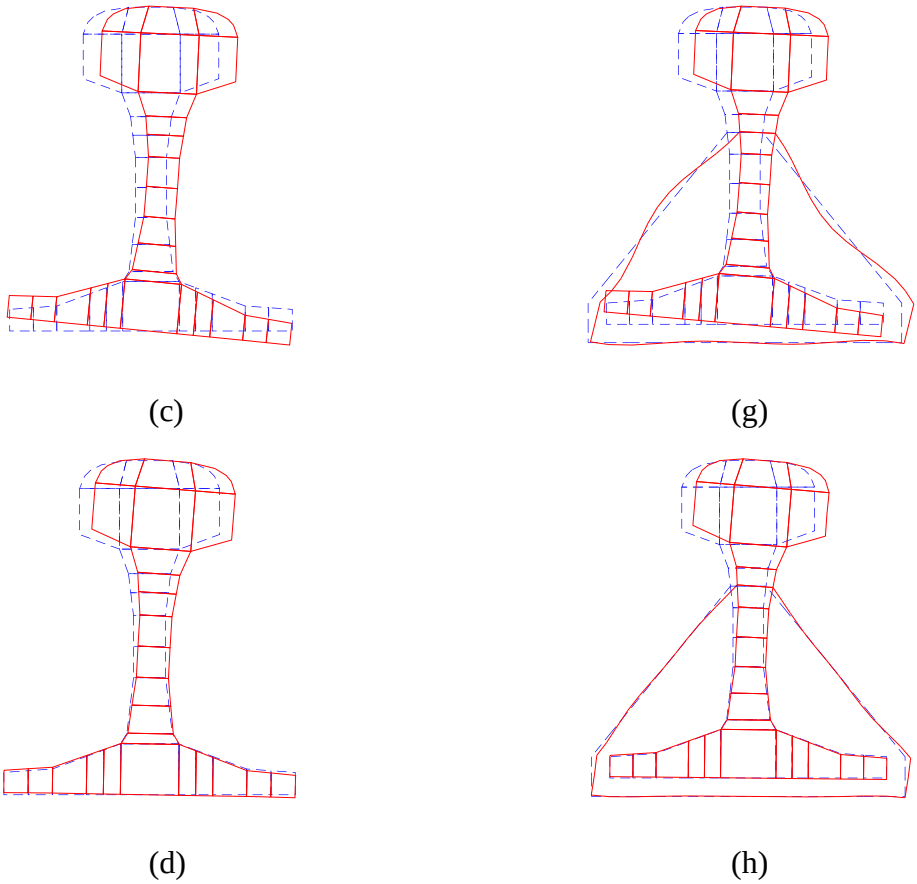

Figure 6 Examples of rail deflected shapes (exaggerated amplitude) for lateral excitation of the rail head. Left: rail without shield: (a) 250 Hz; (b) 500 Hz; (c) 1000 Hz; (d) 2000 Hz. Right: rail with shields fitted: (e) 250 Hz; (f) 500 Hz; (g) 1000 Hz; (h) 2000 Hz.

The sound power radiated by the rail fitted with the shields is calculated in the same way as for the bare rail in Section 3. Results are presented in Figure 7 in one-third octave bands for excitation in the vertical and lateral directions. The result in each band is calculated as the average over five frequencies within the band. These results are shown for the rail (with shields) in free space, attached to a rigid ground and above an absorptive ground.

To show the effect of the shields more clearly, the corresponding insertion loss for the various conditions is presented in Figure 8. The insertion loss is the level difference between the sound power in a given frequency band without the rail shield and with it installed. This difference is independent of the amplitude of the rail vibration (which, as has been seen, is unaffected by the presence of the shields). In these graphs a positive result indicates the noise is attenuated by the shields. For both excitation directions, the rail shields increase the noise at low frequency (negative insertion loss) due to the vibration of the shields, whereas the noise is attenuated at higher frequencies. Again, the results from the rail attached to a rigid ground and above an absorptive ground can be combined following the method proposed in [19]. The resulting insertion losses are also shown in Figure 8.

For the vertical direction, Figure 8(a), the rail shields lead to an increase in noise at low frequency, and a reduction in noise above 300-400 Hz. The combined results in the presence

of the ground follow similar trends to those for the rail in free space but the insertion loss is reduced above 1 kHz. Above 500 Hz the insertion loss for the combined results in the presence of the ground is between 4 dB and 11 dB.

For the lateral excitation, Figure 8(b), the insertion loss results are similar for each set of boundary conditions. The shield system has little influence on the sound radiation of the rail below 250 Hz, but above this frequency it again gives significant reductions. The insertion loss for the combined results in the presence of the ground is between 6 dB and 13 dB above 315 Hz.

Figure 9 compares the insertion loss obtained using the stiff pad with that for the soft pad. These are the combined results in the presence of the ground. For both vertical and lateral directions, the results are very similar for the two stiffnesses of rail pad, although for the vertical direction the insertion loss is 1-2 dB lower for the stiff pad over much of the frequency range. However, it should be emphasised that these results only describe the effect on the rail noise component. The noise radiation from the sleepers and wheels will be unaffected by the rail shields and their contribution will be considered in Section 6.

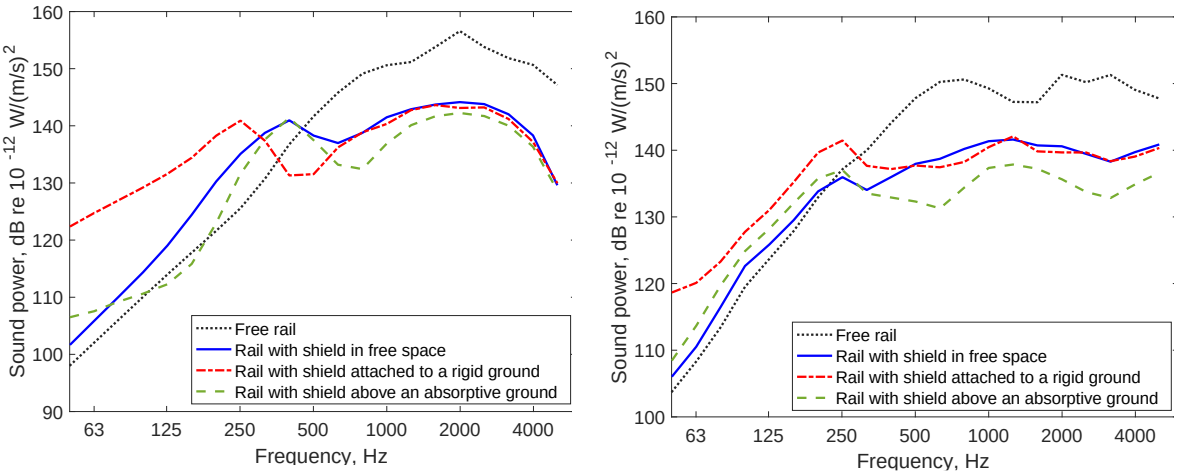

Figure 7 Sound power for a unit mean-square velocity at the excitation point, for the rail fitted with shields. (a) Vertical excitation; (b) Lateral excitation

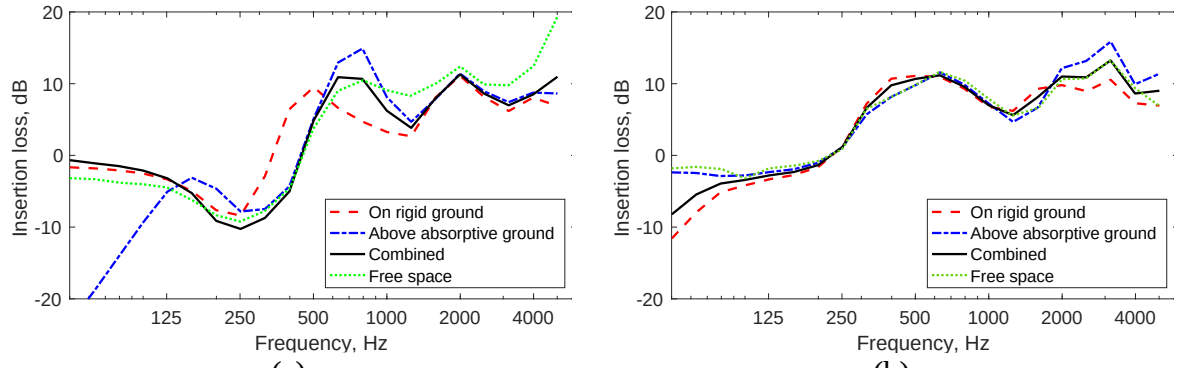

Figure 8 Insertion loss of the rail fitted with shields; results in 1/3 octave bands. (a) Vertical excitation; (b) Lateral excitation

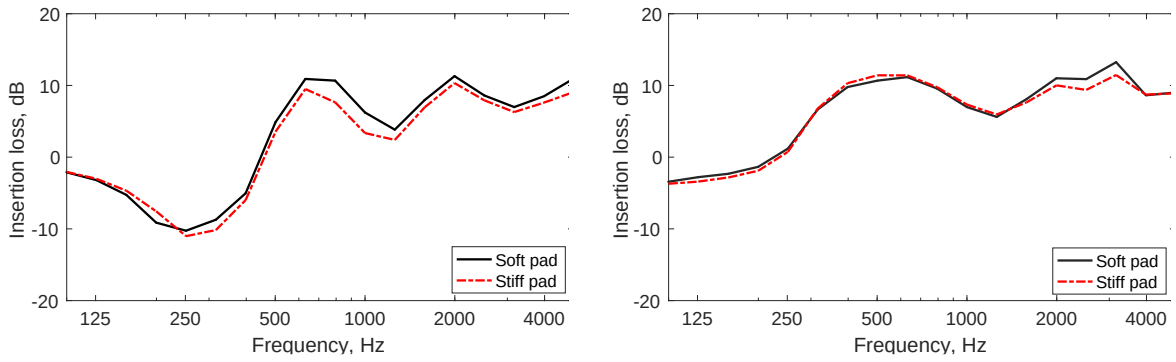

Figure 9 Comparison of insertion losses for the rail shields with soft and stiff rail pads. (a) Vertical excitation; (b) Lateral excitation

4.3 Comparison with measurements

The overall insertion loss results from Figure 9 are compared with the corresponding in-situ measurement data from Dittrich et al. [11] in Figure 10. The measurement data were obtained on a 10 m test track fitted with concrete sleepers by using artificial excitation. The rail shields were installed on one rail of this test track. Two measurement methods were used to obtain vibro-acoustic transfer functions: direct excitation using an impact hammer and a reciprocal method using loudspeaker excitation. For the direct method, the rail was excited with an impact hammer at its centre and the sound pressure was measured at 7.5 m from the track centre at five locations parallel to the track. The average squared pressure spectrum was normalised by the squared excitation force spectrum. The insertion loss was calculated from the change in this ratio due to the introduction of the shields. Similarly, for the reciprocal method, an omnidirectional sound source of known source strength was located at 7.5 m from the track centre and the track acceleration was measured. Again, the results were expressed as an insertion loss. Results were presented in octave bands from 125 Hz to 4000 Hz. At low frequencies, the measurement results for the vertical direction are close to 0 dB due to the influence of the noise from the sleepers, not accounted for in the model. At higher frequencies, for both vertical and lateral excitation, the predictions are higher than the measurement results. This may be associated with differences between the parameters assumed for the shields and porous material and those that apply to the practical installation measured in [11]. The sensitivity of the results to the various assumptions is discussed in Section 5.

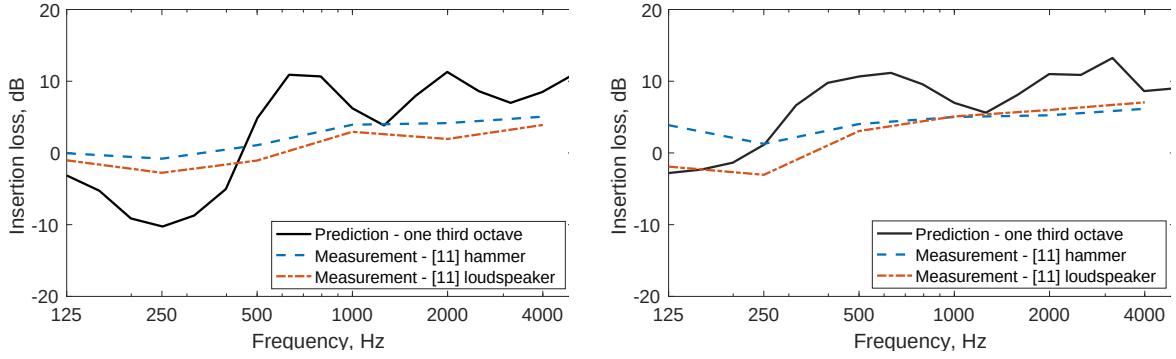

(a) (b)

Figure 10 Insertion loss due to shields for rail on soft rail pads. (a) Vertical excitation; (b) Lateral excitation

5. Parameter study

The rail shield operates by restricting the sound radiation from part of the rail. At the same time, due to mechanical and acoustic coupling with the rail, the shield is caused to vibrate and will itself radiate sound. To investigate the importance of these various mechanisms, the sensitivity of the sound radiation of the rail with shields to various parameter changes is investigated in this section.

5.1 Rigid shield

First, an ideal case of a rigid shield is considered. To model this, the shields are assumed not to vibrate. There is no air or porous material inside the shields; only the acoustic boundary elements on the outer surface are used to model the shield. The rail is vibrating as before.

Results are shown in Figure 11 for the various acoustic boundary conditions in the form of insertion losses relative to the corresponding case for the untreated rail. For the lateral excitation the results are largely independent of the boundary conditions. An insertion loss of around 6 dB is obtained at low frequency due to the reduced area of rail that is radiating. The insertion loss reduces to 0 dB around 1 kHz but above 2 kHz it is more than 5 dB.

For the vertical excitation there is a greater influence of the boundary conditions, especially at low frequency. Although the radiating area is reduced, the shield prevents interference from occurring between the rail head and foot, leading to an increase in the noise for the rail above the absorptive ground, which had the lowest sound power in Figure 2. However, the combined result in the presence of the ground has an insertion loss of around 10 dB at frequencies below 800 Hz. Above 1 kHz the insertion loss for the rail in free space is around 5-8 dB whereas including the effect of the ground it is several dB lower.

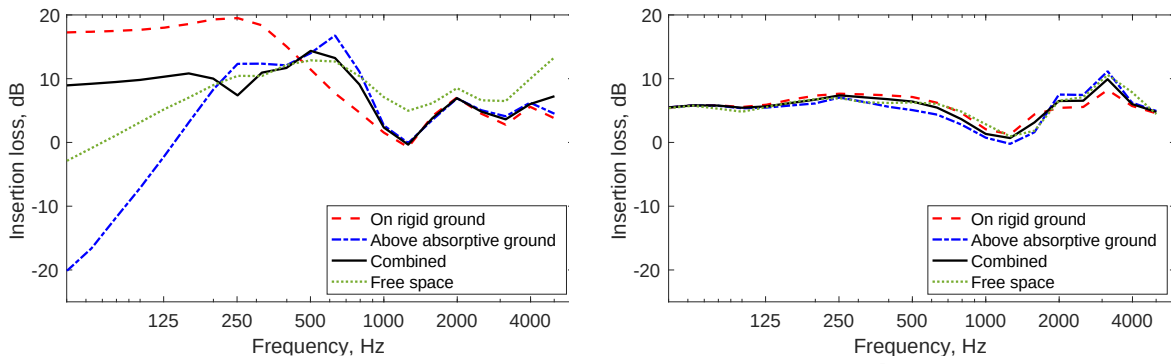

(a) (b)

Figure 11 Insertion loss of a rigid shield for different acoustic boundary conditions. (a) Vertical excitation; (b) Lateral excitation

5.2 Shield with no mechanical coupling

Next, a case is considered in which there is no mechanical coupling between the rail and the shield. The shield is allowed to vibrate but only under the influence of the acoustic loading from the internal fluid. The same mesh is used, as shown in Figure 3.

The insertion loss for this case is presented in Figure 12 and compared with those for the original shield and the rigid shield. This and subsequent results correspond to the combined effect of including the ground. Removing the mechanical coupling generally has adverse effects on the insertion loss compared with the original shield in the whole frequency range and for both directions. The results closely follow those for the rigid shield above 630 Hz for the vertical direction and above 200 Hz for the lateral direction. This indicates that there is some benefit in allowing the shield to vibrate with the rail.

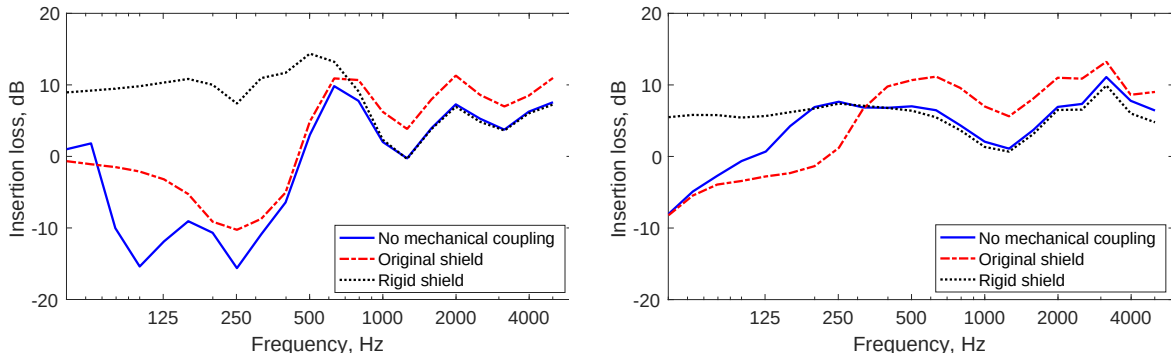

Figure 12 Insertion loss of a shield with no mechanical coupling, compared with original parameters and rigid shield. (a) Vertical excitation; (b) Lateral excitation

5.3 Effect of damping

The effect of the damping treatment applied to the shield is considered by changing the loss factor from the initial value of 0.5 to a lower value of 0.1. The results are shown in Figure 13 for both directions of excitation. The insertion loss follows a similar trend to that for the original parameters, but the benefit of the shield is reduced by around 2 dB for vertical excitation and up to 6 dB for lateral excitation. Thus, with lower damping the shield vibration can be amplified leading to increased noise.

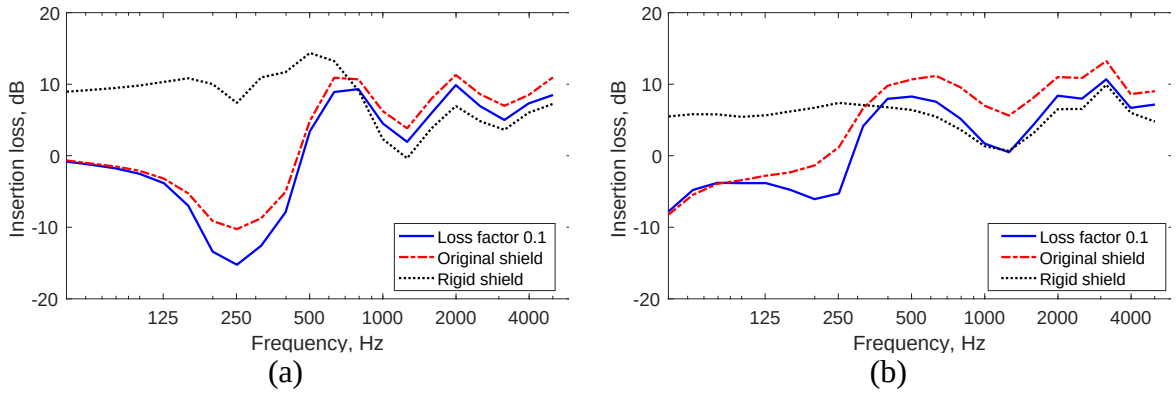

Figure 13 Insertion loss of a shield with reduced damping, compared with original parameters and rigid shield. (a) Vertical excitation; (b) Lateral excitation

5.4 Effect of plate thickness and material

The influence of increasing the thickness of the shield plate from 1 to 2 mm on the insertion loss is shown in Figure 14. For the vertical excitation, the insertion loss is increased by 1-2 dB in most of the frequency range except at around 160 Hz and 250 Hz. For the lateral excitation, the insertion loss is increased below 250 Hz and between 500 Hz and 2000 Hz. The increase of the thickness leads to a reduction in the vibration of the rail shields.

Figure 15 shows the effect of replacing the steel material of the shield by aluminium with a thickness of 1 mm. The insertion loss follows the same trend as the original shield but it is reduced across most of the frequency range. This is caused by an increase in the vibration of the plate compared with the steel one for both vertical and lateral rail vibration, as well as an increase in the sound transmission through the shield.

5.5 Porous material

Finally, Figure 16 presents the effect on the insertion loss of the removal of the porous material. This leads to an increase in the radiation below 250 Hz and above 1600 Hz for vertical excitation, and at all frequencies for lateral excitation, particularly below 1 kHz. The removal of the porous material leads to an increase in the noise level inside the shields and therefore a lower insertion loss is obtained than that of the original shield. The sound pressure level inside the shield is found to increase by an average of 2-3 dB above 250 Hz for both vertical and lateral directions without the absorptive material.

Overall, therefore, it can be seen that the original parameters selected for the shield mostly give the best performance at higher frequencies. An improvement is possible by using a thicker plate but the effect is relatively small.

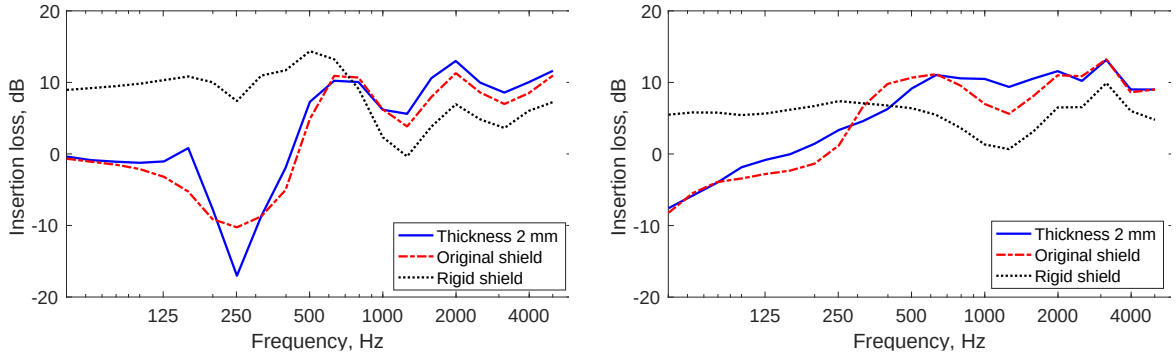

Figure 14 Insertion loss of a shield with increased thickness, compared with original parameters and rigid shield. (a) Vertical excitation; (b) Lateral excitation

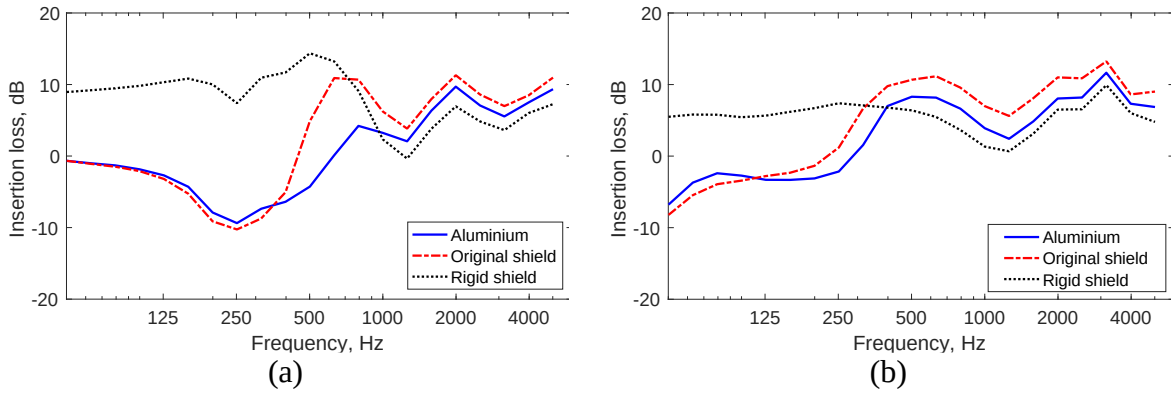

Figure 15 Insertion loss of aluminium shields, compared with original parameters and rigid shield. (a) Vertical excitation; (b) Lateral excitation

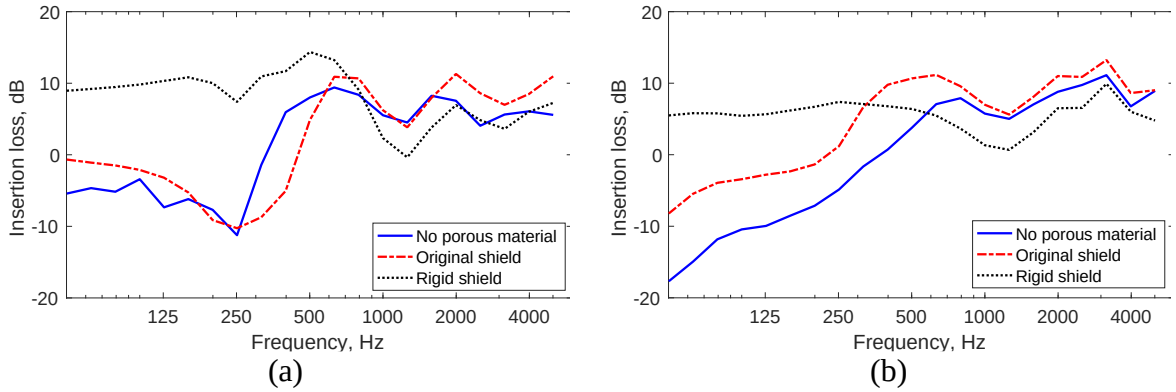

Figure 16 Insertion loss of a shield with no porous material, compared with original parameters and rigid shield. (a) Vertical excitation; (b) Lateral excitation

6. Effects of rail shields on the sound radiation from the track

To assess the effect of the rail shields on train pass-by noise, the TWINS model [15] is used to predict the sound radiated by the wheels, rails (from vertical and lateral vibration) and sleepers. Two different nominal train types [31], a freight train, and a high-speed train, are selected and tracks with the same soft and stiff rail pads as in the former sections have been used. The properties of the trains are listed in Table 3 and the properties used to model the track are listed in Table 4. To give an indication of overall noise reductions, typical measured roughness spectra are used in the predictions. These are shown and compared with the ISO 3095 limit spectrum [38] in Figure 17. These are combined roughness spectra based on the rail roughness measured on a high-speed ballasted track from [39] and typical wheel roughness spectra for wheels with K-block brakes and disc brakes [40].

Table 3 Train type used in TWINS models for assessment of rail shields

Train	High speed train	Freight train
Wheel model	TGV	BA308

Radius (mm)	455	461
Wheel load (kN)	50	100
Vehicle length (m)	26	20
Number of wheelsets per vehicle	4	4
Roughness	Disc	K-block
Speed (km/h)	250	100

Table 4 Track properties used in the TWINS models for assessment of rail shields

		Vertical	Lateral
Rail	Bending stiffness	6.42 MNm^2	1.07 MNm^2
	Damping loss factor	0.02	0.02
	Shear factor	0.4	0.4
	Mass per unit length	60 kg/m	
	Cross receptance factor	-7 dB	
Pad	Stiffness (soft pad)	150 MN/m	25 MN/m
	Stiffness (stiff pad)	800 MN/m	66 MN/m
	Damping loss factor	0.2	0.2
Sleeper	Mass (half sleeper)*	150 kg	
	Spacing	0.6 m	
Ballast	Stiffness**	105 MN/m	35 MN/m
	Damping loss factor	1.0	2.0

*: flexible sleeper model is used for the vertical direction

**: frequency dependent stiffness is used for vertical direction

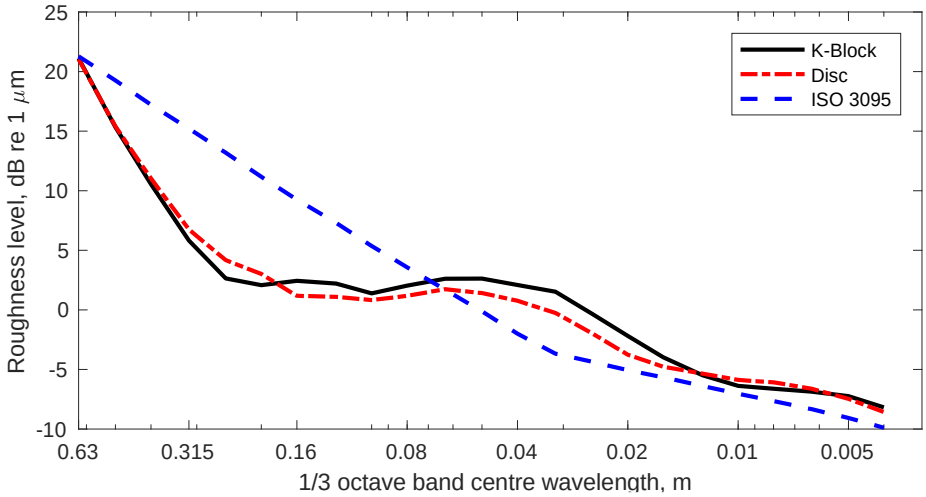

Figure 17 Combined roughness used for the two types of the train

The results are expressed as the sound power for one wheel and the corresponding track vibration and are shown in one-third octave bands. The sound power of the different components for the two types of train are presented in Figure 18 for the track with soft rail pads. The sleeper is the main source of noise below 160 Hz, the rail is the most significant

source in mid frequency range, whereas the wheel contributes the highest sound power at high frequencies.

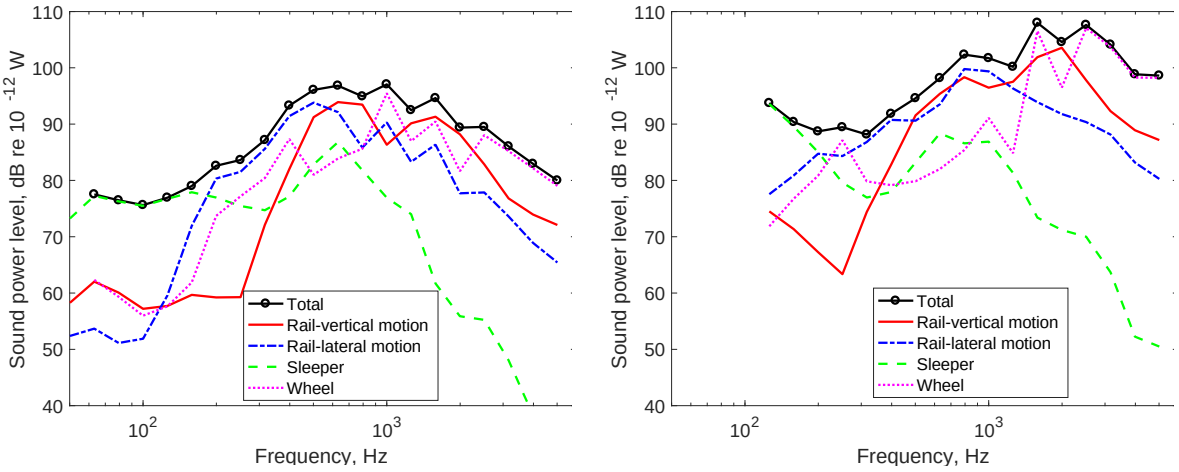

Figure 18 Sound power of the different components for the two train types. (a) Freight train; (b) High-speed train

To predict the noise level with the rail shields, the insertion losses due to the rail shield are applied to the vertical and lateral components of the rail radiation. The wheel and sleeper components are assumed to be unaffected and the new total noise spectrum is calculated by summing the contributions. By comparing this with the total results in Figure 18, the overall insertion loss of the rail shields is obtained. These results are shown in Figure 19 for both soft and stiff rail pads. The insertion loss is around 0 dB below 315 Hz, where the sleeper is the dominant noise source, and above 2500 Hz, where the wheel dominates the noise. In the mid frequency region where the rail noise dominates, the insertion loss for the track with soft pads is larger than that for the track with stiff pads. The noise reduction is no more than 5 dB at any frequency for the track with stiff pads whereas it rises to a peak of 6-8 dB for the track with soft pads.

From the sound power spectra with and without shields, it is found that the overall A-weighted rolling noise for the freight train is reduced by 3.1 dB(A) for the track with soft rail pads and 1.7 dB(A) for the track with stiff pads. For the high-speed train the corresponding overall noise reductions are 1.7 dB(A) and 0.9 dB(A), which are smaller due to the greater contribution of the wheel noise at high frequency.

The results from the different parameter variations considered in Section 5 are shown in the form of the overall insertion loss spectrum in Figure 20 for the track with soft rail pads. Generally, again, the rail shields have limited effect below 200 Hz, where the sleeper is the dominant noise source, and negligible reduction at high frequencies (above 2.5 kHz) where the wheel is the most significant noise source.

Each parameter change relative to the original parameters leads to a loss of performance apart from the increased thickness. A reduction in loss factor can have a considerable detrimental effect on the performance especially at around 200 Hz. Changing the material from steel to aluminium, the noise reduction is less than the original shield parameters, especially between

400 Hz and 800 Hz. If the mechanical coupling is suppressed, the track radiation is reduced at around 250 Hz, but there is about 3 dB more noise than with the original shield parameters between 800 Hz and 1250 Hz. The removal of the porous material causes more noise from the track below 400 Hz for the two train types, and up to 1 dB more noise across all frequencies up to 2 kHz. An increase in the shield thickness, however, has a positive effect on the noise reduction below 2 kHz. The overall noise reduction is around 0.2 dB(A) better than that from the original shield parameters.

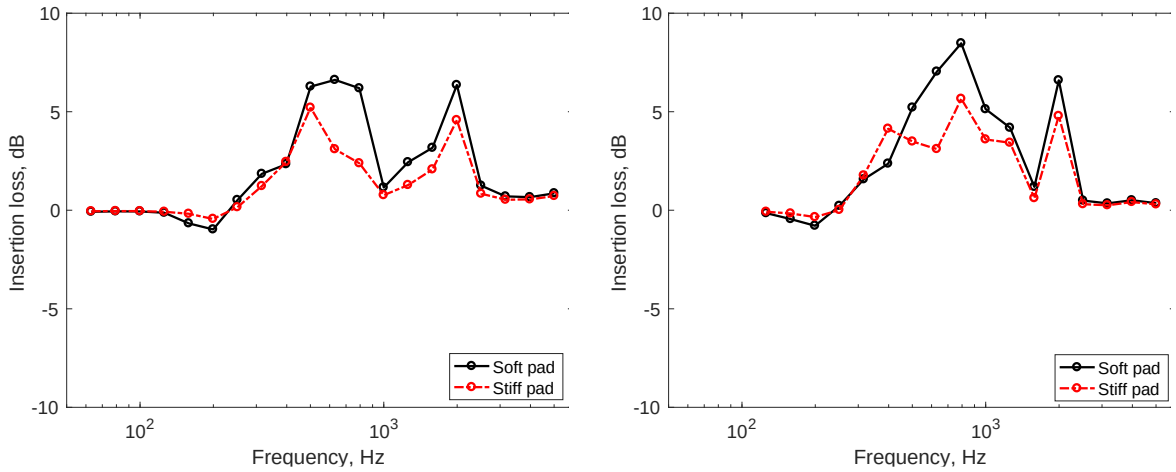

Figure 19 Insertion loss of the total rolling noise for the tracks with soft pad and stiff pad by using the original rail shield parameters. (a) Freight train; (b) High-speed train

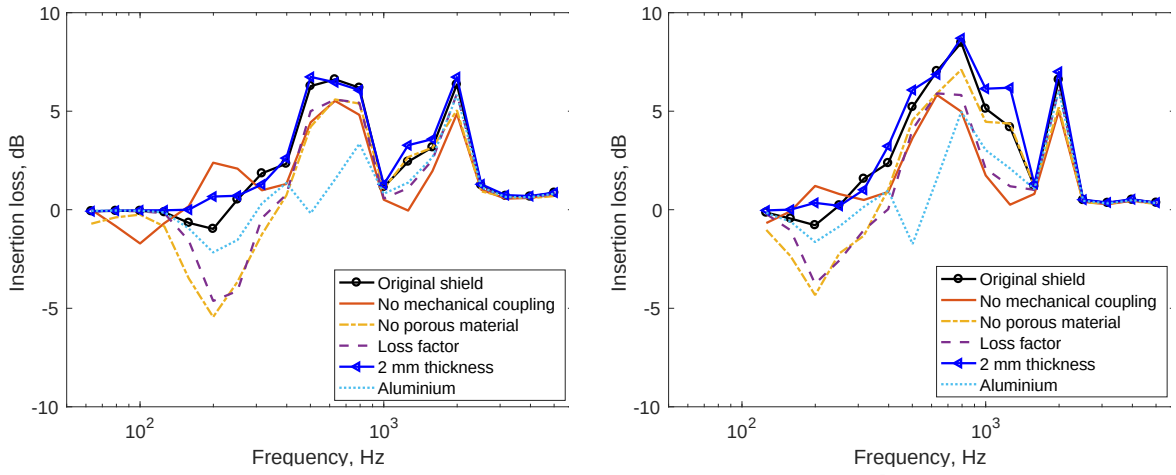

Figure 20 Overall insertion loss of rolling noise for the two train types by using the rail shields with different sets of parameters. (a) Freight train; (b) High-speed train

7. Conclusions

The effect of rail shields on railway rolling noise is investigated by a combination of the TWINS software and numerical predictions. The sound radiation of a rail fitted with an acoustic shield including a layer of porous material is studied numerically by using a 2.5D finite element

and boundary element approach. The shield is shown to have no effect on the track decay rate but modifies the acoustic radiation of the rail. The acoustic effects of the proximity of the sleepers and the ballast are also considered. The rail shields increase the noise at low frequency, but they reduce the noise at high frequency. The stiffness of the rail pad has only a small effect on the insertion loss caused by the rail shield.

The sensitivity of the results to various parameters describing the shield is investigated. The mechanical coupling between the rail and rail shield is shown to be beneficial for the insertion loss. The application of a damping treatment to the shield is also beneficial. The inclusion of the porous material within the shield can increase the insertion loss, especially for the lateral excitation.

The effect of the rail shields with these different parameters on overall rolling noise has also been investigated. The rail shields have a limited effect at low frequency where the sleeper is the dominant noise source, and negligible reduction at high frequency where the wheel dominates the noise. However, in the mid frequency region where the rail is the dominant source, the noise reductions are more significant. The overall A-weighted noise levels are reduced by 2-3 dB for a track with soft rail pads, and 1-2 dB for a track with stiff pads.

References

1 D.J. Thompson. Railway noise and vibration mechanisms, modelling and means of control. Elsevier, Oxford, 2009.

2 M. Beier, T. Lölgen, M. Starnberg. Innovative measures for reducing noise radiation from track. *11th International Workshop on Railway Noise*, Uddevalla, Sweden, In Notes on Numerical Fluid Mechanics and Multidisciplinary Design, 126, 173-180, 2015.

3 D.J. Thompson, P-E. Gautier, 2006, A review of research into wheel/rail rolling noise reduction. Proceedings of the Institution of Mechanical Engineers, Part F (Journal of Rail and Rapid Transit) 220, F4, 385-408, 2006.

4 E. Scossa-Romano, J. Oertli, Rail dampers, acoustic rail grinding, low height noise barriers: a report on the state of the art, Report produced by Swiss National Railways (SBB) on behalf of UIC, October 2012.

5 D.J. Thompson, C.J.C. Jones, T.P. Waters, D. Farrington. A tuned damping device for reducing noise from railway track. Applied Acoustics, 68(1), 43-57, 2007.

6 C. Gramowski, P. Suppin, Impact of rail dampers on the mainline rail roughness development, in: D. Anderson, et al. (Eds) Proceedings of 12th International Workshop on Railway Noise, Terrigal, Australia, 12-16 September 2016, Notes on Numerical Fluid Mechanics and Multidisciplinary Design 139, 367-374, 2018.

7 G. Squicciarini, M.G.R. Toward, D.J. Thompson, 2015, Experimental procedures for testing the performance of rail dampers. Journal of Sound and Vibration, 359, 21-39, 2015.

8 B. Asmussen, D. Stiebel, P. Kitson, D. Farrington and D. Benton. Reducing the noise emission by increasing the damping of the rail: results of a field test. *9th International Workshop on Railway Noise*, Munich, Germany, in Notes on Numerical Fluid Mechanics and Multidisciplinary Design 99, 229-235, 2008.

9 G. Koller, M.T. Kalivoda, M. Jaksch, M. Muncke, T. Oguchi, Y. Matsuda. Railway noise reduction technology using a damping material. *10th International Workshop on Railway*

Noise, Nagahama, Japan, in Notes on Numerical Fluid Mechanics and Multidisciplinary Design 118, 159-166, 2012.

10 P. Huber, J.-D. Liengme and G. Koller. Rail shielding-influence on noise emission and rail vibration. 12th *International Workshop on Railway Noise*, Terrigal, Australia, 2016.

11 M. Dittrich, E. Jansen and C. Czolbe. Characterisation of the effect of rail web shielding. 13th *International Workshop on Railway Noise*, Ghent, Belgium, 2019.

12 D.J. Thompson. Experimental analysis of wave propagation in railway track. Journal of Sound and Vibration, 203(5), 867-888, 1997.

13 D.J. Thompson. Wheel-rail noise generation, part III: rail vibration. Journal of Sound and Vibration, 161(3), 421-446, 1993.

14 D. Kostovasilis, D.J. Thompson, M.F.M. Hussein. A semi-analytical beam model for the vibration of railway tracks. Journal of Sound and Vibration, 393, 321-337, 2017.

15 D.J. Thompson, B. Hemsworth, N. Vincent. Experimental validation of the TWINS prediction program for rolling noise, Part 1: description of the model and method. Journal of Sound and Vibration, 193, 123-135, 1996.

16 D.J. Thompson, P. Fodiman, H. Mahé, Experimental validation of the TWINS prediction program for rolling noise, part 2: results. Journal of Sound and Vibration, 193(1), 137-147, 1996.

17 C.J.C. Jones, D.J. Thompson, Extended validation of a theoretical model for railway rolling noise using novel wheel and track designs. Journal of Sound and Vibration 267(3), 509-522, 2003.

18 X. Zhang, G. Squicciarini, D. Thompson. Sound radiation of a railway rail in close proximity to the ground. Journal of Sound and Vibration, 362, 111-124, 2016.

19 X. Zhang, D. Thompson, E. Quaranta, G. Squicciarini. An engineering model for the prediction of the sound radiation from a railway track. Journal of Sound and Vibration, 461, 114921, 2019.

20 X. Zhang, D. Thompson, G. Squicciarini. Sound radiation from railway sleepers. Journal of Sound and Vibration, 369, 178-194, 2016.

21 X. Zhang, D. Thompson, H. Jeong, G. Squicciarini. The effects of ballast on the sound radiation from railway track. Journal of Sound and Vibration, 399, 137-150, 2017.

22 C.M. Nilsson, J. Ryue, and C.J.C. Jones, Manual for WANDS 2.2 Wavenumber domain software for solids and fluids, University of Southampton, 2010.

23 C.M. Nilsson, C.J.C. Jones, D.J. Thompson, J. Ryue. A waveguide finite element and boundary element approach to calculating the sound radiated by railway and tram rails. Journal of Sound and Vibration, 321, 813-836, 2009.

24 J. Ryue, S. Jang, D.J. Thompson. A wavenumber domain numerical analysis of rail noise including the surface impedance of the ground. Journal of Sound and Vibration, 432, 173-191, 2018.

25 W. Sun, D. Thompson, M. Toward, Z. Zeng. Modelling of vibration and noise behaviour of embedded tram tracks using a wavenumber domain method, Journal of Sound and Vibration 481, 115446, 2020.

26 Y. Zhao, X. Li, Q. Lv, H. Jiao, X. Xiao, X. Jin. Measuring, modelling and optimising an embedded rail track, Applied Acoustics 116, 70-81, 2017.

27 N. Vincent, D.J. Thompson. Track dynamic behaviour at high frequencies. Part 2: experimental results and comparisons with theory. Vehicle System Dynamics Supplement, 24, 100-114, 1995.

28 D.J. Thompson, N. Vincent. Track dynamic behaviour at high frequencies. Part 1: theoretical models and laboratory measurements. Vehicle System Dynamics Supplement, 24, 86-99, 1995.

29 X. Zhang, D. J. Thompson, Q. Li, D. Kostovasilis, M. G. R. Toward, G. Squicciarini, J. Ryue. A model of a discretely supported railway track based on a 2.5D finite element approach. Journal of Sound and Vibration, 438, 153-174, 2019.

30 J.S. Theyssen, A. Pieringer, W. Kropp. The influence of track parameters on the sound radiation from slab tracks, in G. Degrande et al. (Eds.): Proceedings of 11th International Workshop on Railway Noise, Uddevalla, Sweden, 9-13 September 2013. Notes on Numerical Fluid Mechanics and Multidisciplinary Design 150, 90–97, 2021.

31 X. Zhang, D. Thompson, J. Ryue, H. Jeong, G. Squicciarini, M. Stangl. The sound radiation of a railway rail fitted with acoustic shielding. *25th International Congress on Sound and Vibration*, Hiroshima, Japan, July 2018.

32 H. Jeong. A numerical investigation of noise mitigation for railway track. PhD thesis, University of Southampton, 2018.

33 T. Deng, X. Sheng, H. Jeong, D.J. Thompson. A two-and-half dimensional finite element/boundary element model for predicting the vibro-acoustic behaviour of panels with poro-elastic media. Journal of Sound and Vibration, 505, 116147, 2021.

34 J.F. Allard and N. Atalla, Propagation of sound in porous media. Wiley: Chichester, 2nd edition, 2009.

35 H.A. Schenck. Improved integral formulation for acoustic radiation problems. The Journal of the Acoustical Society of America, 44, 41-58, 1968.

36 C.M. Nilsson, J. Ryue, C.J.C. Jones. Theory Manual for WANDS 2.1 Wavenumber-domain FE-BE Software for Structures and Fluids. University of Southampton, 2010.

37 EN 15461:2008+A1:2010. Railway applications. Noise emission. Characterization of the dynamic properties of track selections for pass by noise measurements. European Committee for Standardization, Brussels.

38 ISO 3095:2013 Acoustics - Railway applications - Measurement of noise emitted by railbound vehicles. International Organization for Standardization, Geneva.

39 D. Thompson, G. Squicciarini, J. Zhang, I. L. Arteaga, E. Zea, M. Dittrich, E. Jansen, K. Arcas, E. Cierco, F. X. Magrans, A. Malkoun, E. Iturritxa, A. Guiral, M. Stangl, G. Schleinzer, B. M. Lopez, C. Chaufour, J. Wandell. Assessment of measurement-based methods for separating wheel and track contributions to railway rolling noise. Applied Acoustics, 48-62, 140, 2018.

40 G. Squicciarini, M.G.R. Toward, D.J. Thompson, C.J.C. Jones. Statistical description of wheel roughness. Proceedings of 11th International Workshop on Railway Noise, Uddevalla, Sweden, 9-13 September 2013, Notes on Numerical Fluid Mechanics and Multidisciplinary Design 126, 651-658, 2015.